COMPARISON OF DESIGN GUST AND TURBULENCE LOADS PRESCRIBED IN CERTIFICATION SPECIFICATIONS ON A LONG-RANGE TRANSPORT CONFIGURATION

V. Handojo
DLR Institute of Aeroelasticity, Bunsenstr. 10, 37073 Göttingen, Germany

M. Zimmer
DLR Innovation Center for Small Aircraft Technologies (INK), Department of Aeroelasticity, Campus-Boulevard 97, 52074 Aachen, Germany

M. Kruse
DLR Institute of Aerodynamics and Flow Technology, Lilienthalplatz 7, 38108 Braunschweig, Germany

Summary

This work discusses three approaches for gust/turbulence load calculations prescribed in the certification specifications (CS23 and CS25) of the European Union Aviation Safety Agency (EASA): *quasi-steady load factor*, *dynamic discrete gust*, and *continuous turbulence approach*. Underlying gust and turbulence loads are calculated in MSC.Nastran in combination with a long-range transport configuration, featuring a high aspect ratio of 12.0. Under the requirement of considering aircraft elasticity in all approaches, wing bending moment results exhibit very good agreement throughout all calculations. In the context of the wing torsion moments, deviations caused by the fundamental differences in the approaches become apparent. Due to the absence of structural oscillations, the load factor approach generates the smallest amplitudes, followed by the discrete gust, and finally the continuous turbulence approach. In the latter case, the relation between a low mode damping ratio and high turbulence loads is elaborated. For structural sizing in early design stages, the deviation in the torsion moments are not expected to yield significant differences in the load-carrying wing masses. Nevertheless, the impact of aircraft elasticity on the quasi-steady gust loads are found to be crucial. Hence, the research suggests aircraft elasticity to be considered as early as possible during the aircraft design process. This finding gains in significance for flexible configurations, such as the reference aircraft.

1. INTRODUCTION

In the process of aircraft design, calculations of design flight loads are a crucial aspect, since they yield information about the required structural properties and drive the resulting mass. One important category of design flight loads are gust encounters. To calculate the latter, certification specifications of the European Union Aviation Safety Agency describe three approaches (sorted from simple to more advanced):

The first one is the load factor approach following Pratt et al. [1] (as described in CS23.341 of the Amendment. 4 [2]). In this case, the aircraft is assumed to be rigid. By considering global parameters such as the aircraft wing loading and lift slope, an equivalent gust load factor is derived. Using this load factor, equivalent gust loads can be calculated in a quasi-steady simulation.

The second approach comprises discrete 1-cosine gusts (CS25.341(a) [3]). In doing so, the aircraft elastic modes, flight mechanics, unsteady aerodynamics, as well as control systems have to be considered, and dynamic simulations are mandatory. Besides, sufficient gust gradients ranging from 9 m to 107 m have to be considered, so that a wide frequency range on the aircraft is excited.

The third one is the continuous turbulence approach (CS25.341(b) [3]). The turbulence loads are calculated based on the energy content of the aircraft response in the frequency domain. For this purpose, the von-Kármán turbulence spectrum is considered, and the identification of transfer functions with respect to the load quantities of the aircraft are necessary. Analogous to the discrete gust approach, aircraft elasticity, flight mechanics, and control system are to be taken into account.

In the conceptual design stages of larger aircraft (CS25 category), the load factor approach is commonly used to quickly calculate gust loads. In preliminary design stages, dynamic 1-cosine gust simulations are preferred. For the certification however, loads from the discrete gust simulations as well as continuous turbulence approach are necessary. At this point, the research question arises:

> How comparable are the gust/turbulence loads from each approach, and if there are differences, what and how severe would the expected consequences be in the structural design?

In doing so, the focus of the investigation lies on wing loads.

2. REFERENCE AIRCRAFT AND ITS MODELING

To perform the investigations regarding the gust/turbulence loads, a reference aircraft is considered. Subsection 2.1 gives a brief overview of the aircraft configuration, Subsection 2.2 describes its aeroelastic modeling that is necessary for load calculations, and Subsection 2.3 gives a brief explanation of the design process used to structurally optimize the aircraft.

2.1. Reference aircraft

The reference aircraft is a long-range configuration with a backward swept wing and predominantly composite structure, see FIG 1. Its design originates from the German LuFo project INTELWI [4], and TAB 1 lists a few key parameters of the aircraft. As a remark: in the project INTELWI, the initial wing aspect ratio is 12.4, and a variation of the aspect ratio ranging from 12.0 to 13.2 was conducted. For this work, the aspect ratio 12.0 – which is already relatively high – is considered. Hence, it is expected that aeroelastic effects are significant for the loads.

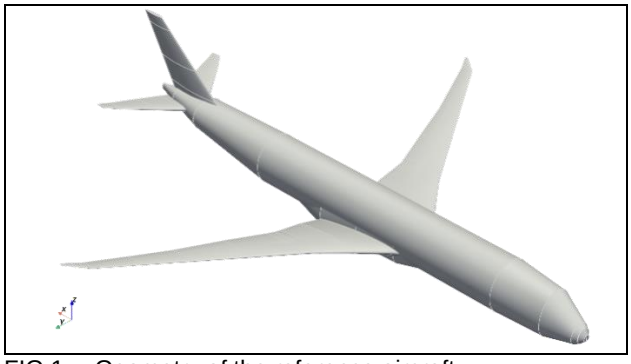

FIG 1. Geometry of the reference aircraft

TAB 1. Key parameters of the reference aircraft

Parameter	Value
Wing reference area	338.5 m²
Wing span	63.8 m
Mean aerodynamic chord	7.33 m
Wing aspect ratio	12.0
Operating empty mass	115 000 kg
Maximum zero fuel mass	167°000°kg
Maximum take-off mass	220 000 kg
Design cruise speed	170 m/s EAS / Mach 0.86
Design dive speed	195 m/s EAS / Mach 0.93
Service ceiling	13106 m (43000 ft)

2.2. Aeroelastic modeling

The aeroelastic models of the reference aircraft for MSC.Nastran are generated and optimized using the in-house design process cpacs-MONA [5].

The primary structure of the lifting surfaces is modeled with shell elements for the skins, spars and ribs, as well as with bar elements for the stiffeners. The fuselage is modeled using beam elements, and the engine pylons are represented by bar elements. FIG 2 shows the FE model of the reference aircraft, where the shell elements for the fuselage and nacelles are for illustration only. Furthermore, the leading and trailing edge of the lifting surfaces are visualized.

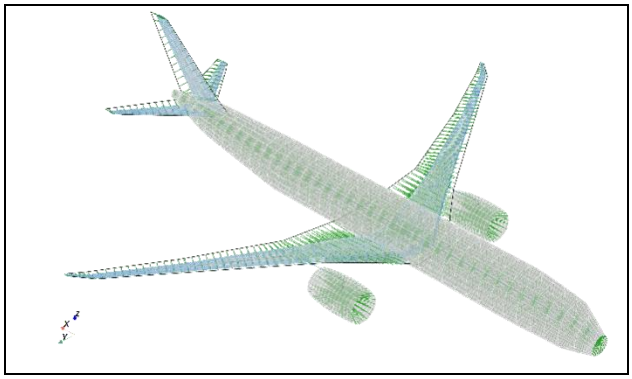

FIG 2. FE model of the reference aircraft, primary structure in blue, rigid element in green

The total mass of the aircraft comprises structural masses, secondary masses, systems, as well as fuel and payload depending on the mass configuration.

For the load calculations, the stiffness and mass properties of the aircraft are condensed onto load reference axis (LRA) nodes, since the global properties of the aircraft are of interest. FIG 3 shows the LRA nodes, as well as nodes at the leading and trailing edge of the lifting surfaces. The latter are connected rigidly to the LRA nodes and used for the splining of the aerodynamic forces.

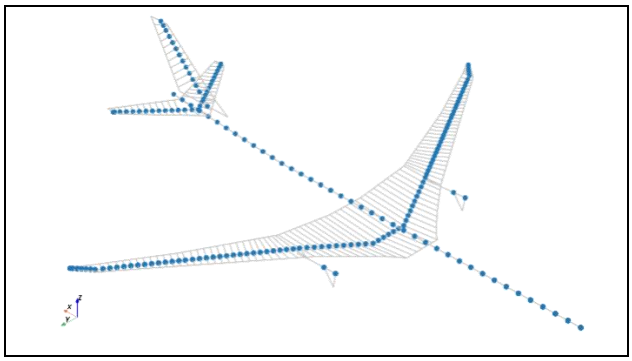

FIG 3. Condensed model of the reference aircraft

The aerodynamic forces are modeled with the vortex lattice method (VLM) [6] for the quasi-steady cases and with the doublet lattice method (DLM) [7] for the unsteady simulations. More details on VLM and DLM can be found in the reference by Voß [8]. The aerodynamic effects of the fuselage are represented by a slender body element, which is based on the subsonic wing-body interference theory [9]. All of the mentioned aerodynamic methods are based on the potential theory and implemented in MSC.Nastran [10]. Furthermore, a correction for the twist and camber of the lifting surfaces are included. FIG 4 shows the aerodynamic model of the reference aircraft with the slender body element as well as the corresponding interference body for the fuselage.

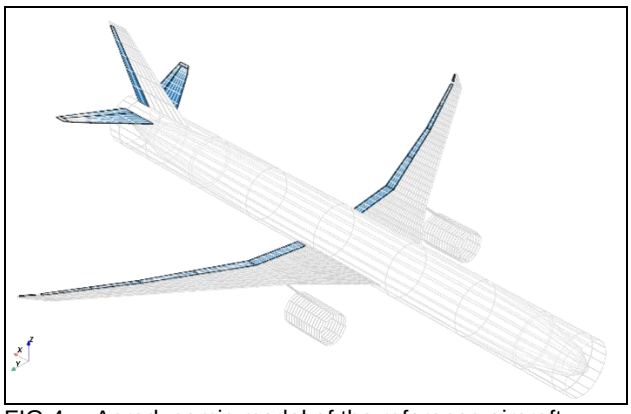

FIG 4. Aerodynamic model of the reference aircraft, control surfaces indicated in blue

2.3. Design process

To obtain initial stiffness and mass properties for the structure, a preliminary sizing for the fuselage beam, stiffener elements as well as skin thicknesses on the lifting surfaces is carried out within cpacs-MONA.

With the pre-sized models, a total of 948 maneuver and 126 gust cases are simulated using MSC.Nastran. In doing so, following aspects are considered:

- six mass configurations ranging from the operating empty mass to the maximum take-off mass,
- for maneuvers: six altitudes between sea level and service ceiling,
  for gusts: three altitudes between sea level and crossover altitude, where the design cruise speed and the design Mach number are reached simultaneously,
- for maneuvers: pull-up, push-down, roll and yaw cases at various airspeeds between the design maneuvering speed and the design dive speed,
  for gusts: seven gust gradients ranging from 9 to 107 m at the design cruise speed,
- no load alleviation function is implemented.

The loads resulting from the simulations are then post-processed to narrow down the number of load cases which are relevant for the structural optimization of all lifting surfaces.

The structural optimization itself is carried out with MSC.Nastran, with the minimum mass as objective function. Subsequently, a second optimization with the aileron effectiveness as objective function is carried out. If the first optimization already yields a positive aileron effectiveness, then no changes are made in the second optimization. However, if the resulting aileron effectiveness is negative, only an increase in the material thicknesses is made in the second optimization.

The steps with the loads analysis and structural optimization are carried out iteratively, until a mass convergence criterion is met. A more detailed description of cpacs-MONA can be found in the reference by Klimmek et al. [5]. Finally, the pitch stability and aileron effectivity of the aircraft are checked for the whole flight envelope. Therefore, these criteria are checked for all combinations of mass configurations and flight conditions. Thus, a feasible design for subsequent analyses is guaranteed.

3. GUST LOAD CALCULATION METHODS

As mentioned in Section 1, there are three methods of gust/turbulence load calculation prescribed in the certification specifications:

- load factor approach following Pratt et al.,
- dynamic simulation of discrete 1-cosine gusts,
- continuous turbulence approach.

The following subsections give an overview of the respective methods. Furthermore, since the load results shown in Section 4 are calculated using MSC.Nastran, relevant aspects regarding the respective simulations are also elaborated.

3.1. Load factor approach

The quasi-steady load factor approach is described in CS23.341 of the Amendment 4 [2] and based on the NACA Report 1206 by Pratt and Walker [1]. The report introduces a formula to calculate a load factor which is supposed to represent the peak accelerations emerging during a discrete 1-cosine gust encounter:

$$(1) \qquad n_z = 1 \pm \frac{k_g \rho_0 U_{de} V_{EAS} c_{Z\alpha}}{2(W/S)},$$

where the gust alleviation factor k_g is defined as:

$$(2) \qquad k_g = \frac{0.88\,\mu_g}{5.3+\mu_g},$$

and the mass ratio μ_g is defined by:

$$(3) \qquad \mu_g = \frac{2(W/S)}{\rho c_{ref} c_{Z\alpha} g},$$

with:

n_z	: total load factor [-]
U_{de}	: gust velocity [m/s EAS]
ρ_0	: air density at sea level [kg/m³]
ρ	: air density at considered altitude [kg/m³]
W/S	: wing loading at the current mass [N/m²]
c_{ref}	: reference chord [m]
g	: gravitational acceleration [m/s²]
V_{EAS}	: equivalent airspeed [m/s EAS]
$c_{Z\alpha}$	: lift slope of the overall aircraft [1/rad].

In the derivation of Equation (1), following assumptions (which differ from the 1-cosine gust requirements) are applied [1]:

- the aircraft is rigid,
- the aircraft can perform heave, but not pitch motion (nevertheless, the load-mitigating effect of pitching motion is included in the gust alleviation factor k_g [1]),
- the gust gradient (half wavelength) is 12.5 times chord length.

For the simulation with MSC.Nastran, the quasi-steady aeroelastic solution sequence SOL144 is used. The conducted steps are as follows:

1) Steady trim calculation for the 1.0 g level flight condition (zero pitch velocity, zero pitch acceleration). The variables are angle of attack and deflection of the horizontal stabilizer. The latter as well as the lift slope are recorded.

2) Calculation of the gust load factors according to Equation (1) with the lift slope obtained in step 1.
3) Two subsequent quasi-steady simulations (one for the positive gust, one for the negative gust) with the calculated load factors from step 2, the horizontal stabilizer deflection from step 1 and zero pitch velocity. The variables are angle of attack and pitch acceleration.
   The applied setting implies that no control surface is moved prior to and during the gust encounter. Furthermore, since the combination of the horizontal stabilizer deflection from step 1 and the gust load factors from step 2 yield an imbalance in the pitching moment, the pitch acceleration is set free, so that the imbalance is compensated by the inertial loads of the aircraft.

The steps listed above are carried out for all considered mass configurations and all flight conditions.

In CS23, no passage regarding mandatory consideration of aircraft elasticity in load calculations is found [2]. On backward swept wing configurations such as the reference aircraft however, the structural elasticity has a load alleviation effect due to the bending-torsion-coupling.

In Equation (1), the effect appears in the form of a smaller lift slope that in turn decreases the incremental gust load factor. In the quasi-steady simulations described in step 3, the bending-torsion coupling decreases the local lift slopes around the wing tip, so that the lift distribution is shifted towards the wing root, which in turn decreases the bending moment.

In applying the quasi-steady load factor approach, there are three possible ways to neglect or include the aircraft aeroelasticity described above, see TAB 2. Its influence on the loads is shown in Subsection 4.3.

TAB 2. Possible ways to include aircraft aeroelasticity in gust load factor approach

Label	**Calculation of gust load factor with … aircraft**	**Simulation with MSC.Nastran with … aircraft**
Rigid	rigid	rigid
Semi-flexible	rigid	flexible
Flexible	flexible	flexible

3.2. Discrete 1-cosine gust approach

The discrete 1-cosine gust approach is described in CS25.341(a). For the calculation of the gust loads, dynamic simulations including the aircraft elastic modes, flight mechanics, unsteady aerodynamics and control system are mandatory [3].

Compared to CS23, the reference gust velocities for the discrete gust approach in CS25 are different. Additionally, a flight profile alleviation factor – that is a function of the aircraft design masses, service ceiling and the considered altitude – is introduced and used to mitigate the gust amplitude. In total, the gust design velocity is defined by [3]:

$$U_{ds} = U_{ref} F_g \left(\frac{H}{107\ \mathrm{m}}\right)^{1/6}, \quad (4)$$

with:
U_{ds} : design gust velocity [m/s EAS]
U_{ref} : reference gust velocity [m/s EAS]
F_g : flight profile alleviation factor [-]
H : gust gradient [m].

In the gust simulations, sufficient gust gradients ranging from 9 m to 107 m (30 ft to 350 ft) have to be considered [3]. FIG 5 shows exemplary gust profiles. Note that the gust amplitude is proportional to the sixth root of the gust gradient.

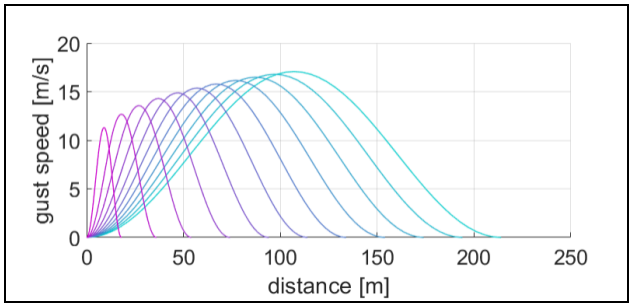

FIG 5. Exemplary discrete 1-cosine gust profiles

For the simulation with MSC.Nastran, following steps are necessary:

1) Dynamic simulation with the dynamic aeroelastic solution sequence SOL146. In this case, since the simulation is carried out in the frequency domain, only incremental loads are obtained (if there is no gust, then the loads are zero).
2) Steady trim calculation for the 1.0 g level flight condition with SOL144 to obtain the static loads.
3) Superposition of the dynamic loads from SOL146 and the static loads from SOL144 to yield the total loads acting on the aircraft:

The steps listed above are carried out for all considered mass configurations, all flight conditions and all gust gradients. Furthermore, step 1 and 3 apply for positive as well as negative gusts. For the wing, mainly vertical gusts are sizing relevant. However, if any aircraft component is sized by lateral or oblique gusts, respective gust simulations have to be conducted [3].

FIG 6 shows exemplary responses of the wing root bending moment M_x and torsion moment M_y to 1-cosine gusts.

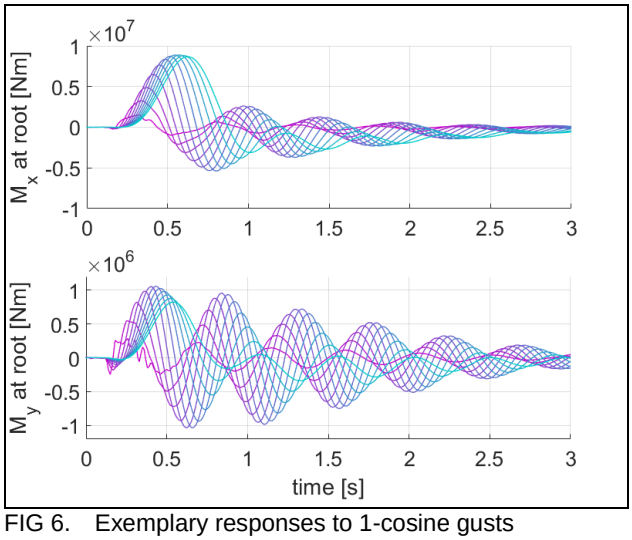

FIG 6. Exemplary responses to 1-cosine gusts

3.3. Continuous turbulence approach

The continuous turbulence approach is elaborated in CS25.341(b). Similar to the discrete gust approach, a consideration of the aircraft elastic modes, flight mechanics, unsteady aerodynamics and control system is mandatory [3].

The turbulence limit loads are defined by a superposition of the static loads during 1.0 g level flight and the turbulence loads:

(5) $$P_{limit}=P_{1g}\pm U_\sigma \bar{A},$$

where:

(6) $$\bar{A}=\sqrt{\int_0^\infty [|TF(f)|^2 \Phi_{rms=1}(f)]df},$$

with:
P_{limit} : turbulence limit loads in general
P_{1g} : 1.0 g static loads in general
U_σ : limit turbulence intensity [m/s TAS]
$TF(f)$: transfer function in general
$\Phi_{rms=1}(f)$: normalized turbulence power spectral density [1/Hz].

The term $\bar{A}$ approximately describes the magnitude of the aircraft response to unit turbulenfce and is unique for every transfer function $TF(f)$. The transfer function itself describes the frequency response of an observed output quantity (e.g. wing root bending moment, fuselage vertical acceleration). In this case, the vertical wind speed is an input quantity. Since transfer functions are single input single output (SISO) systems, one transfer function is necessary for every output quantity.

The prescribed turbulence spectrum in this approach is the von-Kármán spectrum with a turbulence scale of 2500 ft (762 m) and the following definition of the normalized power spectral density (PSD):

(7) $$\Phi_{rms=1}(f)=\frac{2L_{turb}}{V_{TAS}}\frac{1+\frac{8}{3}\left(1.339\cdot 2\pi f\frac{L_{turb}}{V_{TAS}}\right)^2}{\left(1+\left(1.339\cdot 2\pi f\frac{L_{turb}}{V_{TAS}}\right)^2\right)^{11/6}},$$

with:
$\Phi(f)$: PSD of von-Kárman spectrum [1/Hz],
L_{turb} : turbulence scale [m]
V_{TAS} : true airspeed [m/s TAS]
f : frequency [Hz].

A more general definition of the PSD is written as a function of the normalized frequency $\Omega=\frac{2\pi f}{V_{TAS}}$ [3]. However, since the transfer function results in MSC.Nastran are given in Hz, a conversion of the PSD to a function of the frequency (in Hz) is preferred. FIG 7 shows an exemplary normalized von-Kármán turbulence spectrum. The term normalized spectrum implies that the integral of the PSD is equal to 1.0.

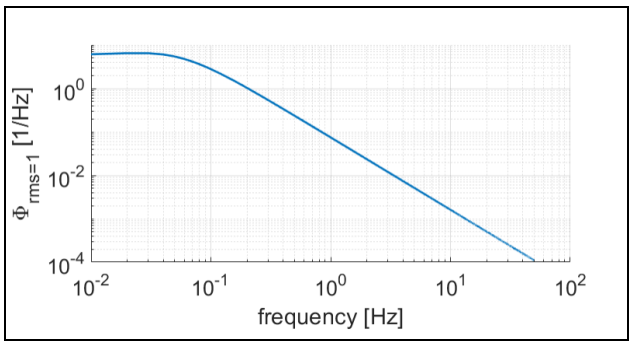

FIG 7. Exemplary von-Kármán turbulence spectrum

The considered frequency range for the calculations of the transfer functions is capped at 50°Hz, since the contribution to the energy content of the frequencies above is comparatively small. Furthermore, a white noise excitation with unit turbulence is applied in the corresponding calculations in MSC.Nastran.

With Equation (5) and (6), limit load values for each load quantity can be obtained. However, those limit loads do not always emerge at the same time, e.g. the maximum wing root bending moment and torsion do not necessarily appear simultaneously. Hence, to generate 2D load envelopes e.g. for the wing root, a correlation between the bending moment and the torsion (or shear force and torsion) is necessary. The correlation can be interpreted as scalar product between two quantities and is defined by:

(8) $$\rho_{1,2}=\frac{\int_0^\infty [\Phi_{rms=1}(f)\ real(TF(f)TF'_2(f))]df}{\bar{A}_1\bar{A}_2}$$

with:
$\rho_{1,2}$: correlation between load quantity 1 and 2
$H'(f)$: complex conjugated transfer function

FIG 8 illustrates exemplary magnitudes and correlations of turbulence loads in a 2D envelope. ΔM_x and ΔM_y indicate that those are incremental loads due to turbulence, not the total loads acting on the aircraft.

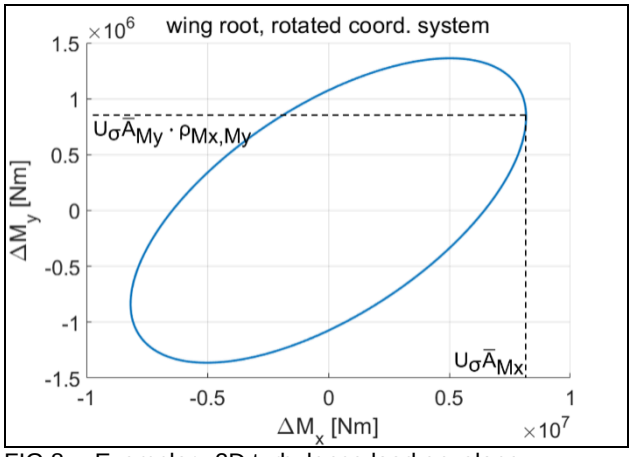

FIG 8. Exemplary 2D turbulence load envelope

In the context of the load evaluation, an octagon can be drawn around the ellipsoidal load envelope, and the tangential points can be considered as design loads [3]. In Subsection 4.2 however, only the load envelopes are shown and compared to the other methods, and the step with the octagon and the tangential points is neglected.

For the certification, loads due to vertical and lateral turbulence have to be considered. For the wing – analogous to the discrete gust approach – the largest loads are expected during vertical turbulence.

4. PARAMETER SPACE AND LOADS RESULTS

Subsection 4.1 lists the parameter space considered for the gust/turbulence loads analysis, and Subsection 4.2 compares the load results of the three approaches. Subsection 4.3 quantifies the influence of the aeroelasticity on the gust loads from the load factor approach, and Subsection 4.4 elaborates the contribution of the elastic modes to the turbulence loads.

4.1. Parameter space

The following passages explain the selection of the parameter space, and TAB 3 gives an overview of the simulation parameters.

For the load calculations, two mass configurations are considered: the operating empty mass (OEM), and one maximum take-off mass (MTOM) configuration with maximum payload. The largest negative wing loads are expected to be reached at OEM, while MTOM – especially with maximum payload and thus a heavy fuselage – is expected to yield the largest positive wing loads.

Three flight conditions are taken into account: design cruise speed at sea level, 4000 m (FL131) and 8000 m (FL262). The latter is approx. the altitude where the design cruise speed VC and the design cruise Mach number MC are reached simultaneously.

In general, VC is selected since it provides the highest dynamic pressures for the prescribed gust velocities at full amplitude. Above VC, the gust amplitudes are linearly reduced until they are halved at VD. Thus, the largest gust loads are expected to emerge at VC.

Furthermore, at MC above 8000 m, the dynamic pressure decreases with altitude, so that the gust loads at high altitudes are not expected to be sizing relevant for the wing.

In all three gust/turbulence load approaches, positive and negative gusts/turbulences are considered. In the discrete gust approach, a total of 11 gust gradients between 9 m and 107 m are considered, see FIG 5.

All gust and turbulence loads are calculated with the clean aerodynamic configuration, i.e. no airbrake and no high lift device is extended. TAB 3 gives an overview of the parameter space.

In total, there are 12 gusts for the load factor approach, 132 gusts for the discrete gust approach, and six transfer function calculations for the continuous turbulence approach.

TAB 3. Parameter space for the simulation

Parameter	Quantity	Value
Mass configuration	2	OEM MTOM, max. payload
Flight condition	3	VC, 0 m VC, 4000 m VC, 8000 m
Gust direction	2	Vertical upward and downward
Aerodynamic configuration	1	No airbrake, no high lift device

4.2. Load results

The comparison of the gust/turbulence load results from the three approaches comprises the bending moment envelopes over the wing half-span as well as 2D load envelopes at selected cross-sections. FIG 9 visualizes the local coordinate systems on the wing as well as the monitoring stations where the 2D load envelopes are shown.

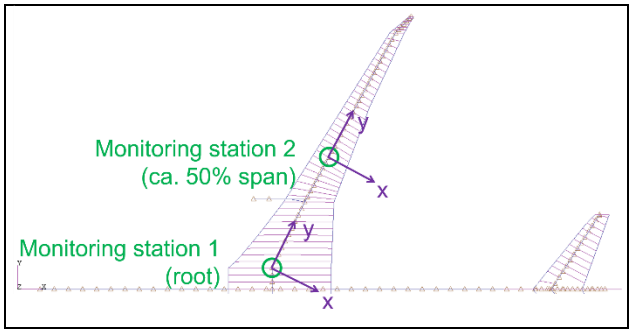

FIG 9. Local coordinate systems on the wing and monitoring stations for the 2D load envelopes

FIG 10 shows the wing bending moment envelopes. As a remark: the results from the load factor approach are obtained using the semi-flexible case mentioned in TAB 2. This means, the gust load factors (step 2 in Subsection 3.1) are calculated with parameters of the rigid aircraft, and the quasi-steady simulations (step 3 in Subsection 3.1) are carried out with the elastic aircraft.

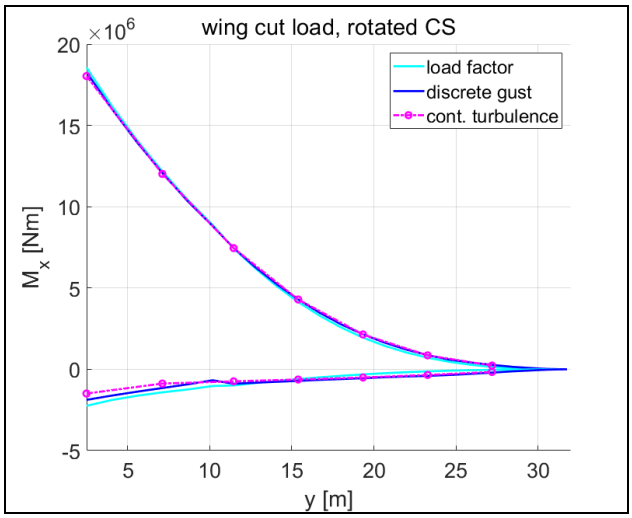

FIG 10. Comparison of wing bending moment envelopes

It is apparent that all three approaches yield a very good agreement of the wing bending moment envelope. At the root, the load factor approach yields the largest M_x value, while the maximum M_x of the discrete gust approach is 1.6% smaller, and that of the continuous turbulence approach is 2.9% smaller. For the minimum M_x – which is reached with the OEM mass case – the load factor approach yields the largest magnitude in the section between the root and the engine attachment (y = 10 m). This aspect indicates that the engine has an alleviation effect on M_x in the dynamic approaches with discrete gusts and continuous turbulence. In the outer part of the wing (y > 20 m), the envelope of the load factor approach is visibly smaller compared to the other two approaches. This is caused by the absence of the loads resulting from structural oscillations which emerge in the two dynamic approaches.

With regard to the torsion moment M_y, differences are visible, as can be seen in the 2D envelopes at the wing root, see FIG 11. The smallest span between the minimum and maximum M_y is found in the load factor approach, since there are only static loads acting on the aircraft – and no loads due to oscillations. Furthermore, loads during the 1.0 g trim conditions are also visualized for a better overview of the discrete gust as well as continuous turbulence approach, since the incremental loads are superposed with the corresponding trim loads.

In the discrete gust approach, the engine pitch mode is excited the gust encounters, which in turn evokes larger M_y peak values. The largest M_y peak values are, however, found in the continuous turbulence approach. A significant contribution to this phenomenon comes from the combination of the low damping ratio of the engine mode and the continuous excitation of the turbulence. A more detailed explanation regarding this aspect is given in Subsection 4.4.

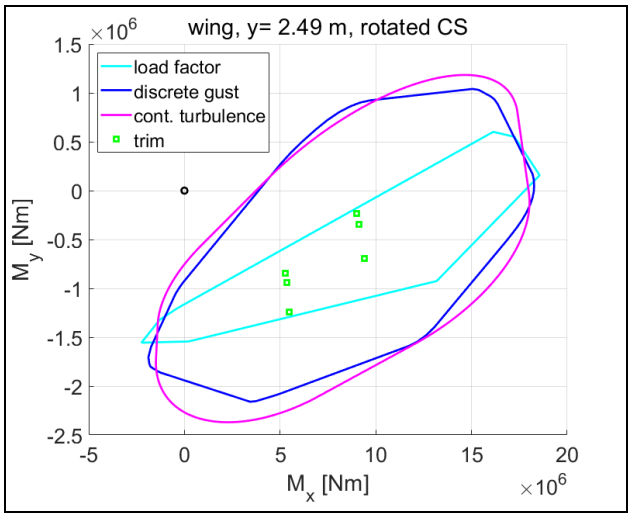

FIG 11. Comparison of 2D load envelopes at wing root

At approx. 50% span, similar trends are visible: the peak values of M_y from the load factor approach are the smallest, and those from the continuous turbulence approach are the largest, see FIG 12. Judging by the rounder load envelopes from the discrete gust and continuous turbulence approach, it is apparent that the correlation between M_x and M_y is slightly lower compared to that at the wing root.

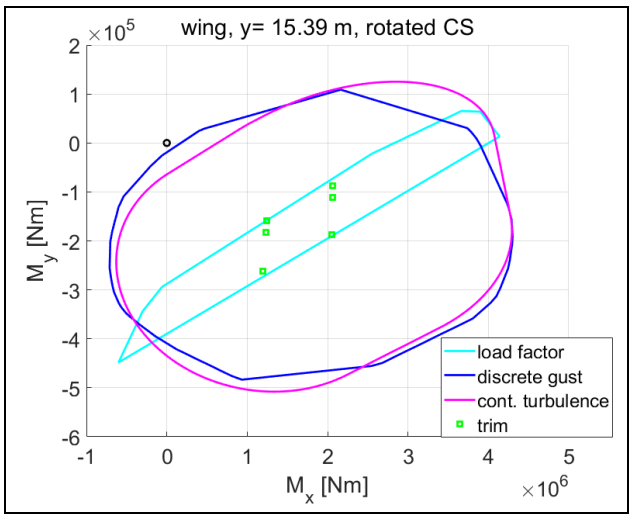

FIG 12. Comparison of 2D load envelopes at 50% span

4.3. Influence of aeroelasticity

In the early stages of an aircraft design process, information regarding the structural elasticity might not be available yet. In this case, first gust load calculations using the load factor approach with a rigid aircraft is an adequate solution. Nevertheless, it is advisable to consider the aircraft aeroelasticity in the load calculations as early as possible – at least for configurations with a high aspect ratio wing such as the reference aircraft.

To underline the influence of the aircraft aeroelasticity, two comparisons among the cases listed in TAB 2 are made. The first one concerns the calculation of the gust load factors (step 2 in Subsection 3.1). TAB 4 shows an exemplary comparison of the lift slope values and the gust load factors (at MTOM) between the rigid and flexible aircraft.

TAB 4. Exemplary comparison of lift slope values and gust load factors

Mass case, flight condition	**Lift slope**	**Gust load factor**
MTOM, VC at 0 m	rigid: 5.547 flexible: 5.109	rigid: 1±1.008 flexible: 1±0.942
MTOM, VC at 4000 m	rigid: 5.926 flexible: 5.405	rigid: 1±1.132 flexible: 1±1.045
MTOM, VC at 8000 m	rigid: 6.995 flexible: 6.212	rigid: 1±1.235 flexible: 1±1.110

The second comparison deals with the resulting gust loads (step 3 in Subsection 3.1). FIG 13 shows the wing bending moment envelopes of the quasi-steady gust loads. It is apparent that the load envelope of the rigid case is vastly different compared to the semi-flexible and flexible case. At the wing root, the maximum bending moment of the rigid case is 37.8% higher in contrast to the semi-flexible case. On the flexible case, the maximum bending moments are only slightly smaller compared to the semi-flexible case, with a difference of –5.0% at the root.

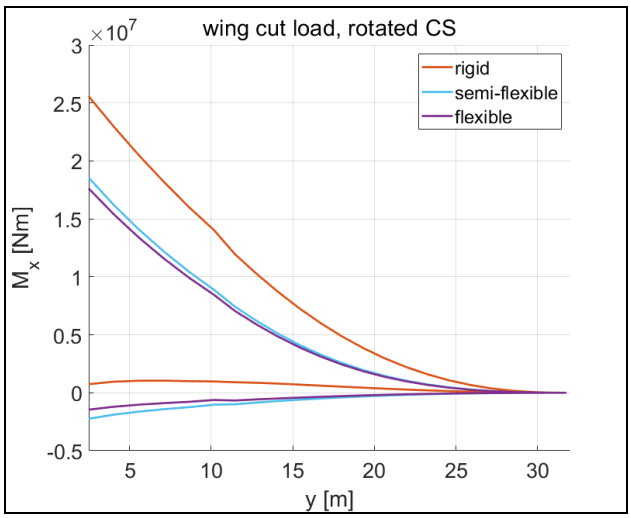

FIG 13. Comparison of bending moment envelopes

To verify the large differences between the rigid and semi-flexible case, an additional comparison of the spanwise lift distribution (MTOM, VC at 8000 m, load factor 2.235) is shown in FIG 14. It is apparent that the outer wing section of the semi-flexible case generates significantly less lift. This phenomenon is two result of two effects:

- As the wing generates lift, it bends upward. Due to the bending-torsion coupling, the local angle of attack in the outer section is smaller (compared to that at the root), so that the local lift is decreased.
- The camber of the wing profile creates a nose-down moment, which twists the wing and in turn decreases the local angle of attack as well as the local lift. This effect is most pronounced in the outer wing section.

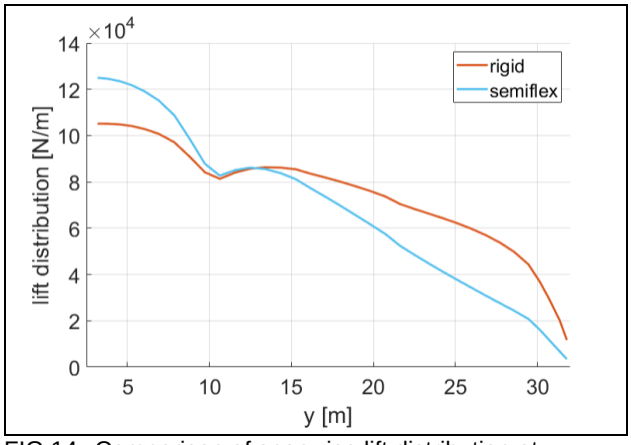

FIG 14. Comparison of spanwise lift distribution at maximum gust load factor

Furthermore, the rigid case creates 7.3% more total lift force on the wing. The latter is equal to the integral of the spanwise lift distribution. As a remark: the semi-flexible case yields a larger angle of attack, hence the fuselage and HTP create more lift (or less downforce), while the wing generates less lift. With this additional comparison, the large differences in the wing bending moments between both cases seem plausible.

In total, it can be concluded that:

- For the calculation of the gust load factors, the aircraft aeroelasticity only plays a minor role (in the form of the smaller lift slope).
- In the quasi-steady simulations with the calculated gust load factors however, the inclusion of the aircraft aeroelasticity is crucial to avoid obtaining too large loads.

4.4. Contribution of modes to turbulence loads

The magnitude of the turbulence loads $\bar{A}$ as defined in Equation (6) is obtained with theoretical integral limits set to [0., ∞] Hz. In the calculation with MSC.Nastran, the integral limits are set to [0., 50.] Hz, see Subsection 3.3. Within that frequency range, each elastic mode has a nominal contribution to the integral value of $\bar{A}$. To narrow down the number of load quantities, the next passages deal with $\bar{A}$ values for the wing root bending moment M_x and wing root torsion M_y of the mass case MTOM, at VC at 8000 m.

To obtain an overview of the mode contributions in the frequency domain, cumulative aircraft responses $\bar{A}_{cum}$ are calculated using cumulative integrals:

$$(9) \qquad \bar{A}_{cum}(f_c)=\sqrt{\int_0^{f_c}[|TF(f)|^2\Phi_{rms=1}(f)]df} \ .$$

Compared to Equation (6), the only change in Equation (9) is the upper limit of the integral is a variable instead of a fixed number. Hence, the result of Equation (9) is a function of f_c instead of a scalar.

FIG 15 shows the cumulative response for the wing root bending moment of $\bar{A}_{cum}(M_x)$. It is apparent that practically the entire response energy to turbulence is contained below 3 Hz, since the curve of $\bar{A}_{cum}(M_x)$ above that frequency is flat. Furthermore, two areas with steeper slopes are found:

- A large one around 0.2 Hz. This slope is evoked by a resonance with the short period mode of the aircraft.
- A smaller one around 1.8 Hz. This slope emerges from a resonance with the first symmetric wing bending mode (with the given mass case and flight condition).

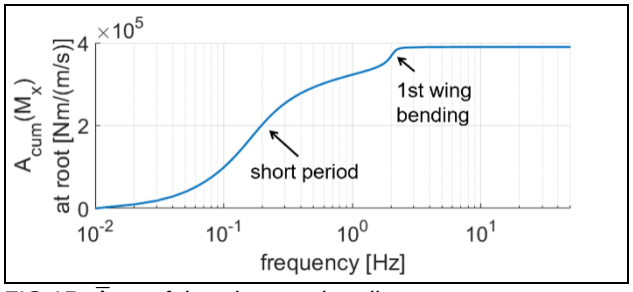

FIG 15. $\bar{A}_{cum}$ of the wing root bending moment

FIG 16 visualizes the cumulative response for the wing root torsion moment of $\bar{A}_{cum}(M_y)$. Similar to M_x, the entire response energy of M_y to turbulence is practically contained below 3 Hz. However, a striking feature of the curve is a very steep slope – almost like a step – around 2.2 Hz. This is caused by a resonance with the symmetric engine pitch mode (with the given mass case and flight condition). Furthermore, the almost vertical slope indicates that the mode has a low damping ratio. For the wing root torsion M_y, the engine pitch mode makes up almost 50% of the response magnitude – it brings $\bar{A}_{cum}(M_y)$ from below 30000 Nm/(m/s) to ca. 55000 Nm/(m/s).

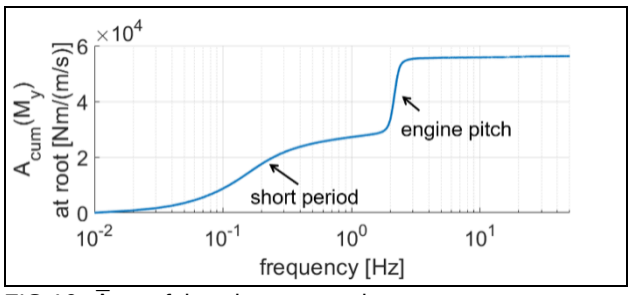

FIG 16. $\bar{A}_{cum}$ of the wing root torsion moment

A remark regarding damping: If the engine mode had an infinitely small damping ratio, a single excitation e.g. of a discrete gust at the resonance frequency would evoke high, but finite peak values of the wing root torsion, and the decay of the oscillation would be very slow. For the discrete gust approach, the design loads would be those finite peak values.

With a continuous excitation such as turbulence however, the peak values of the wing root torsion in the steady-state oscillation would become infinitely high. Hence, for the continuous turbulence approach, the magnitude of the design loads would be infinite – and therefore larger compared to those from the discrete gust approach.

As a conclusion: if there are contributing modes with low damping ratios, the loads from the continuous turbulence approach are expected to be higher compared to those from the discrete gust approach.

5. CONCLUSIONS AND OUTLOOK

5.1. Conclusions

Calculations and comparisons of gust/turbulence loads from three approaches found in the EASA certification specifications have been carried out. In doing so, the aircraft elasticity is considered in the (quasi-steady) load factor approach, and is mandatory for the (dynamic) discrete gust as well as continuous turbulence approach. The reference aircraft is a long-range transport aircraft with a wing aspect ratio of 12.0.

Loads and their impact on the aircraft design

In total, it can be concluded that all three approaches yield a very good agreement in the wing bending moment envelope – as long as the aircraft elasticity is considered in the quasi-steady load factor approach as well. On the other hand, the differences in the torsion moments are larger – especially between the quasi-steady and the dynamic approaches. Furthermore, the minor differences in the torsion moments between the discrete gust and continuous turbulence approach have been discussed.

For the aircraft design, the impact of the loads on the structural mass is an interesting aspect to be addressed. For the first step, a comparison with the maneuver loads (which are not part of this investigation) should be conducted. If the gust/turbulence loads are dominant, the following points are to be considered:

- The inner wing section – which has the largest mass per span – is typically sized by bending moments. Since the bending moment envelopes of the three approaches have a very good agreement, no significant differences in the (bending driven) structural masses are expected. Furthermore, the ratio of magnitude between the maximum bending moment and torsion moment at the root is approx. 10:1 on the reference aircraft. Thus, variations in the torsion loads are only expected to yield minor differences in the structural masses.
- Towards the wing tip, the contribution of the torsion moments in driving the structural mass increases. At the same time, the wing cross-section area decreases, so that the mass per span also diminishes. This means, even if variations in the torsion moments evoke larger differences in the structural masses of the outer wing part, the total wing mass is not expected to be affected significantly.

However, if the wing structure is sized with considerably smaller torsion moments from the quasi-steady approach, the resulting torsional stiffness might be smaller – especially on composite structures with variable laminates. This aspect could in turn lead to deviations in the mode frequencies and flutter behavior.

Nevertheless, for early design stages where not much information about the aircraft is not known yet, the quasi-steady load factor approach proves to be adequate for gust load calculations.

Influence of aeroelasticity on loads

Regarding the effect of aeroelasticity on the loads, quasi-steady gust loads have been calculated with three variants of elasticity. Considering a rigid aircraft, the wing root bending moment is found to be 37.8% larger compared to that on an elastic aircraft. Besides, if the gust load factor is calculated with an elastic aircraft (in the form of elastic lift slope) the load simulation (also with an elastic aircraft) yields a 5.0% smaller bending moment at the wing root. At this point, it can be concluded that the aircraft elasticity should be considered as early as possible in the design process, especially when aeroelastic effects are expected to be significant, as it is the case for the reference aircraft.

5.2. Outlook

To obtain a broader overview of gust/turbulence loads, cases with extended airbrakes can be taken into account. In the airbrake-out configuration, the lift in the mid wing section – where the spoilers are located – is reduced. To maintain the total lift force in the trim condition, the angle of attack increases. Hence, the inner and outer part of the wing generates more lift. In turn, the latter evokes larger (positive) bending moments in the mid wing section. If superposed with the incremental gust/turbulence loads, the total (positive) loads are expected to be larger compared to the clean configuration (airbrake-in).

However, the modeling of spoiler deflections is not trivial, since they induce flow separations which are not covered by panel methods e.g. in MSC.Nastran. At this point, it is advisable to take references from CFD (computational fluid dynamics) simulations into account.

For a comprehensive structural sizing or optimization, further loading conditions such as maneuvers and landing should be considered. This is because different loading conditions are sizing relevant for different parts of the structure.

For structural optimization in MSC.Nastran, sets of nodal loads (distributed loads over the wing span) are required. These can be obtained from the load factor and discrete gust approach (in the latter as time-correlated loads). However, the continuous turbulence approach yields only load envelopes, and no concrete sets of nodal loads. Hence, alternative ways to include turbulence loads in the optimization have to be considered, such as scaling certain load components from the discrete gust approach to match the envelopes from the continuous turbulence approach.

ACKNOWLEDGMENTS

The authors thank the Federal Ministry for Economic Affairs and Climate Action (Bundesministerium für Wirtschaft und Klimaschutz - BMWK) for the funding as part of LuFo VI-1 in the project INTELWI.

REFERENCES

[1] Pratt, K., and Walker, W., "A revised gust-load formula and a reevaluation of v-g data taken on civil transport airplanes from 1933 to 1950," NACA Report No. 1206, 1954.

[2] European Aviation Safety Agency, "CS23 - Certification Specifications for Normal, Utility, Aerobatic, and Commuter Category Aeroplanes - Amendment 4," 2015.

[3] European Aviation Safety Agency, "CS25 - Certification Specifications and Acceptable Means of Compliance for Large Aeroplanes - Amendment 27," 2021.

[4] Wunderlich, T., and Siebert, F., „Optimierung von Steuerflächenausschlägen am hochgestreckten Flügel zur Steigerung der Gleitzahl im Reiseflug," in: 22. DGLR-Fachsymposium der STAB, Berlin, 2022.

[5] Klimmek, T., Schulze, M., Abu-Zurayk, M., Ilic, C., and Merle, A., "cpacs-MONA – An independent and in high fidelity based MDO tasks integrated process for the structural and aeroelastic design for aircraft configurations," in: International Forum on Aeroelasticity and Structural Dynamics 2019, Savannah, GA (USA), 2019.

[6] Katz, J., and Plotkin, A., "Low speed aerodynamics, 2nd ed." Cambridge, UK; New York: Cambridge University Press, 2001.

[7] Albano, E., and Rodden, W., "A Doublet Lattice Method for Calculating Lift Distributions on Oscillating Surfaces in Subsonic Flows," AIAA Journal, vol. 7, no. 2, 1968.

[8] Voß, A., "An Implementation of the Vortex Lattice and the Doublet Lattice Method," DLR-Interner Bericht, DLR-IB-AE-GO-2020-137, 2020.

[9] Giesing, J. P., Kálmán, T. P., and Rodden, W. P., "Subsonic Steady and Oscillatory Aerodynamics for Multiple Interfering Wings and Bodies," Journal of Aircraft, vol. 9, no. 10, 1972.

[10] MSC Corporation, "MSC Nastran 2018.2 - Aeroelastic Analysis User's Guide," 2018.